EDDY CURRENT TESTING OF INCONEL 718 ALLOY – PRELIMINARY STUDY

MATUS GEĽATKO[1], RADOSLAV VANDZURA[1], MICHAL HATALA[1], FRANTISEK BOTKO[1]

[1]Technical University of Kosice, Faculty of Manufacturing Technologies with a seat in Presov, Slovakia

DOI: 10.17973/MMSJ.2025_06_2025050

matus.gelatko@tuke.sk

The calibration process is an important part of the preparation for eddy-current testing (ECT) of different materials and the subsequent creation of identification methodologies, which need to be specifically related to certain probes. The paper describes an experiment focused on the preliminary study of Inconel 718 alloy, during which parameters of three selected probes are evaluated. The main objective is to obtain detailed information about the identification abilities of these probes for evaluated material. The standard penetration depth of eddy currents into the material is calculated based on the conductivity determined using the special conductivity probe, where was found that it is important to measure conductivity for a specific material before the ECT identification. The lift-off effect diagrams are interpreted for all three probes, which represent the base for the understanding of the identification abilities of used probes. Subsequently, suitability assumptions of probes for different applications are expressed.

KEYWORDS

nickel-based alloy, non-destructive testing, eddy-current testing, lift-off, standard penetration depth

1 INTRODUCTION

Demanding requirements on special properties of materials in the modern industry define applications of materials with specific compositions. Nickel-based alloys are traditionally used and experimentally tested within subtractive manufacturing (SM) [De Bartolomeis 2021] and equally within the expanding additive manufacturing (AM) [Mostafaei 2023]. Inconel 718 alloy is characterized by the combination of corrosion resistance, higher strength, exceptional weldability with resistance to cracking after the welding process, and outstanding creep-rupture strength. Common applications include aircraft engine components, turbines, space shuttles, nuclear reactors, or tooling [Inkosas 2025].

With the increased requirements on materials, which are included within special applications, the high quality of final components is indispensable. Non-destructive eddy-current testing (ECT) method can simply identify surface and sub-surface defects, or material characteristics such as density, and residual stresses, and distinguish material structure, with possible automatization, including various probe designs [Machado 2024]. Pereira, D. and Clarke T.G.R. designed an ECT sensor for the detection of cracks in cladding made from Inconel 625 alloy, whereas FEM models were important for proposal and optimization with subsequent experimental verification [Pereira 2014]. A relation of phase angle variation with a damage degree after a static tensile test was made on Inconel 718 alloy, with the expression of phase angle as a function of the damage parameter [Krysztofik 2019]. Superalloy MAR 247 with aluminide coating was the material of interest during the assessment of damage after the force-controlled fatigue tests, with the monitoring of probe resistance and stated optimal accuracy between 165 – 170 kHz excitation frequency [Tytko 2024]. Inconel 625 alloy was applied as the clad layer on the API 5L X65 steel substrate within the study describing the in-line inspection of fatigue crack, using the ECT method [Camerini 2018]. In recent studies, the eddy current testing was applied on various materials made using the Laser Powder Bed Fusion (LPB-F) methods [Spurek 2025], which were on the base of stainless steel [Sun 2023], aluminium [Spurek 2021], or titanium [Farag 2022]. Considering AM nickel-based alloys, artificial defects in subsurface layers of Inconel 738LC alloy were probed using a differential ECT probe, with the evaluation of influencing excitation frequency, lit-off, defects´ parameters, residual heat, and roughness [Guo 2021].

Considering the material base, its composition, manufacturing technology, and its parameters, important material characteristics in the form of electrical conductivity and magnetic permeability are influenced, hence it is necessary to calibrate the used ECT system for a specific material to get the best possible output data of the identification. Studied sources mainly include experiments and calibrations conducted using the specifically designed probes. It is appropriate to express crucial parameters of commercial ECT probes, which will be important for setting subsequent and similar experiments, focused on ECT of Inconel 718 alloy. The described study includes an experiment focused on the preparation of a measurement device and selected probes for the evaluation of Inconel 718 alloy. The possibilities of the evaluation are expressed through the lift-off effect and lift-off diagrams of selected probes, and standard penetration depth calculation in their frequency range, with the subsequent prediction of appropriate setting of ECT parameters for various purposes and selection of suitable probes.

2 MATERIALS AND METHODS

The material selected for the experiment was the nickel-based alloy Inconel 718 (HAYNES® 718), including a higher content of chromium, iron, niobium, and molybdenum. The aluminium and titanium are in the less amount. A percentage of content is included in the following Tab. 1 [Inkosas 2025].

Element	Mass (%)	Element	Mass (%)
Co	≤ 1	Si	≤ 0.35
Fe	19	Ti	0.9
Cr	18	Al	0.5
Bb+Ta	5	C	0.05
Mo	3	C	0.009
Mn	≤ 0.35	Cu	≤ 0.1

Table 1. Chemical composition of nickel-based alloy HAYNES® 718

Experimental measurement included the application of the eddy-current testing device NORTEC 600 (Fig. 1) by Olympus company, working on a principle of electromagnetism.

Figure 1. Nortec 600 device with probes

The main output of the identification is the impedance signal deviation in the form of curves, which can be interpreted in two main regimes. The first Impedance (IMP) regime depicts deviation curves on the vertical axis (reactance – imaginary part of the impedance) and on the horizontal axis (resistance – real part of the impedance), which are numerically expressed with labels VMAX and HMAX, respectively. The second Sweep (SWP) regime depicts signal deviations in the form of peaks (amplitudes) on a vertical axis over time on a horizontal axis, whereas both regimes can be monitored at the same time on the screen of a device. The obtained signal depends on the excitation frequency and can be adjusted, which includes its rotation using the ANGLE (phase angle) function and its intensification or attenuation using the GAIN function [Evident 2025]. Four probes were used for the experiment, three were spot type (two with conical shape) and one was conductivity (Tab. 2) probe. For the reaching of various lift-off distances (distance between a probe and a material), non-conductive plastic shims were used.

Label	Probe	Type	*d* [mm]	*f* [kHz]
A1	INDETEC ndt MTW100.S3.A1 N	Absolute	10	10 - 100
A2	INDETEC ndt RFW20.S3.B1N	Absolute	2	200 - 2000
A3	INDETEC ndt RFW20.S3.B1N	Absolute	2	500 - 5000
C4	OLYMPUS SPO-887L	Conductivity	7.9	60

Table 2. ECT probes selected for experiment

During the experiment, a material was probed using A1 - A3 probes at the lift-off distances of 0.15, 0.30, 0.60, 0.90, and 1.20 mm, whereas VMAX and HMAX were recorded for the evaluation of the lift-off effect for used probes. For the A1 probe, 5 frequencies were selected and for the A2 and A3 probe, 10 frequencies were selected due to their wider frequency range. Standard penetration depth (δ) for the whole frequency range of probes was calculated and the main parameter (electrical conductivity) of the material was obtained using the conductivity probe (C4). It is an important parameter for the planning of a measurement using the ECT method, due to the estimation of the area of a material that will be tested. This depth is defined as an area of the material, where the ECT method can provide reliable measurement outputs, whereas a density of eddy currents is equivalent to 37% of the 100% density on the surface of a material. Several decisive parameters influence this δ and they can be categorized into two groups. The first includes material properties, which are electrical conductivity and magnetic permeability, and the second includes excitation frequency which is related to the used ET probe. The following equation (1) expresses the relation of the mentioned parameters [García-Martín 2011].

$$\delta = \sqrt{\frac{1}{\pi . f . \mu . \sigma}} \tag{1}$$

where f is the excitation frequency, μ is the magnetic permeability and σ is the electrical conductivity. Considering that Inconel 718 alloy is a non-magnetic material, magnetic permeability can be neglected. Hence, electrical conductivity is the key material parameter that influences standard penetration depth. The manufacturer states its value on 1.42% IACS (International Annealed Copper Standard) [Inkosas 2025], but it is appropriate to measure the conductivity of the real material. For this purpose, the fourth conductivity probe (C4) was used. First, it is necessary to calibrate the device and probe before the conductivity measurement. The calibration process includes four main steps, during which the limit conductivity values of known materials are loaded into the device, and during the measurement, the conductivity of probed material is determined based on limit values. As the low-limit material, AW 7075-T6 aluminium alloy was selected. A conductivity value of the data sheet (33.48% IACS) [Matweb 2025] was set on a device, the probe was placed on the specimen and the value was stored. As the high-limit material, CW004A copper alloy was selected, and its conductivity value (101.42%) [Matweb 2025] was stored in the same way. Both steps were repeated similarly but with the application of plastic shim (100 µm) between the probe and both materials. The reason is calibration for the measurement of non-conductive coating thickness.

3 RESULTS

The experimental part includes standard penetration depth calculation of eddy currents into the Inconel 718 alloy within the frequency range of used probes and the evaluation of the influence of lift-off distance on their parameters (reactance and resistance).

3.1 Standard penetration depth calculation

After the successful calibration of the C4 probe, the probe was placed on the Inconel 718 alloy, and a device calculated the conductivity value on 1% IACS. It needs to be mentioned that it is the lowest value that the device interprets, hence it can be less in the case of Inconel 718 material. Such differences in conductivity between a data sheet and a measurement can be caused by variations in the percentage of elements, manufacturing process, and the basic characteristics of evaluated nickel-based alloy, which is naturally low-conductive material, potentially causing higher deviations during the conductivity measurement. Both conductivity values (data sheet and determined) were included in equation (1) and standard penetration depth was calculated for the frequency range of all three probes (A1 - A3). The following Fig. 2 interprets standard penetration depth which can be reached in the Inconel 718 alloy. Maximum depth (6.61 mm) can be

reached using the A1 probe at 10 kHz, whereas the minimum is 2.09 mm at 100 kHz frequency. If the more sensitivity of a measurement is required, probes A2 and A3 are more suitable. A2 probe provides a maximal depth of 1.48 mm at 200 kHz, and it is evident that the selected three probes cannot cover the frequency range between 100 and 200 kHz. The A3 probe can reach 0.93 mm maximal depth at 500 kHz. The minimal standard penetration depth is 0.47 mm at 2 MHz for the A2 probe and 0.30 mm at 5 MHz for the A3 probe, respectively.

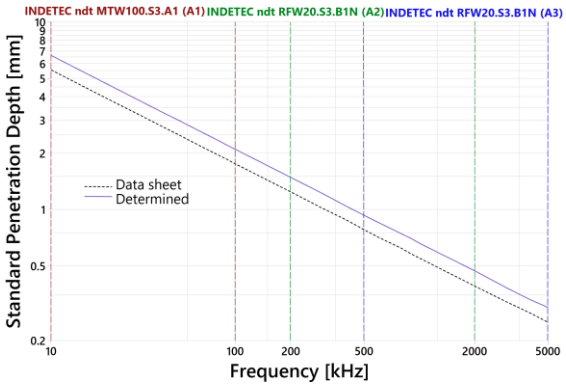

Figure 2. Graph of standard penetration depth

3.2 Lift-off effect evaluation

For the prediction of sensitivity and identification capacities of used probes, signal deviations on the vertical axis (VMAX) and horizontal axis (HMAX) were recorded for selected lift-off distances. The reactance (VMAX) development is interpreted in the following Fig. 3. VMAX variations increase with the lift-off distance in the case of all frequencies within all three probes, but the sense and magnitude are different. For the A1 probe, the VMAX variation increases with the decrease of excitation frequency, whereas 10 and 30 kHz frequencies partially overlap each other and at such set parameters, higher sensitivity can be predicted in their frequency range. The slope of the 100 kHz curve is less steep than in the case of others. The development of curves at A2 and A3 is different. The first mentioned reached the smallest deviation at the lowest frequency (200 kHz), whereas higher frequency curves (1.4 – 2 MHz) tended to deviate in the negative direction and others in the positive direction. Hence, higher sensitivity can be predicted in the case of frequencies with curves deviated further from zero (600 and 800 kHz or 1.8 and 2 MHz) at such set parameters. The curve of the lowest frequency (500 kHz) of the A3 probe reached a negligible deviation at 1.2 mm lift-off and 2.5 – 4 MHz frequency curves deviated in the negative direction. Others deviated to the positive direction with a significant variation of 5 MHz frequency curve with the maximum approx. 5 VMAX at 1.2 mm, which can be predicted as the most sensitive frequency, confirms the increase of sensitivity with the increase of the excitation frequency. Described trendlines are mainly influenced by a design characteristic of probes. Curves of the A1 probe are similar in shape and in a positive direction which is the consequence of a smaller frequency range, where similar sensitivity can be predicted at all frequencies. If the range is wider, such as in the case of A2 or A3 probes where minimal frequencies are in tens of kHz and maximal frequencies are in a few MHz, trendlines direct in both, positive and negative directions, due to the covering of all frequencies for the reliable depiction of curves with their sufficient resolution and without losing limit frequency curves beyond the display level of a measurement device. Mentioned phenomena can be seen in the case of the 5 MHz curve within the A3 probe, which deviated further away from other curves.

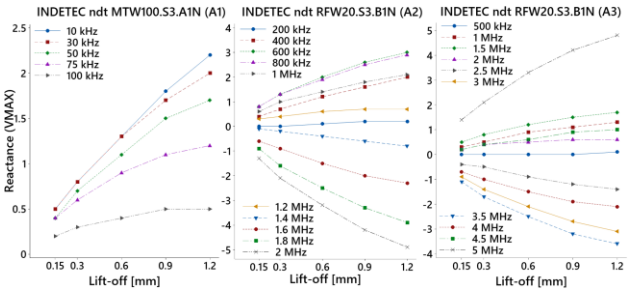

Figure 3. Reactance (VMAX) dependency on lift-off

The curve development of the HMAX parameter based on the variation of lift-off distance was different (Fig. 4). However, HMAX increased with the increase of lift-off, which is a known characteristic of this parameter. During the measurement with the A1 probe, its deviation increased with the increase of the excitation frequency. 10 kHz frequency curve reached only minimal deviation at all lift-off distances; thus, its slope is the most significantly different from others. It can be stated that the lift-off will influence the identification in a greater manner by using the higher frequencies in the case of the A1 probe. A similar trend of curves´ development was observed at the A2 probe, where 200 kHz and 400 kHz frequencies reached deviation in a negative direction, whereas the 600 kHz curve slightly exceeded zero value in a positive direction. A change in a trend occurred above 800 kHz where higher frequencies varied differently with the maximal deviation of 1.4 MHz. Furthermore, 1.2 and 1.6 MHz curves have almost identical transitions. Similarly to the A1 probe, the effect of lift-off will be more influential at higher frequencies of the A2 probe at such parameters of measurement. During the probing with the A3 probe, most frequency curves deviated into the negative direction, whereas the highest magnitude was present between 4 – 5 MHz frequencies. A significant deviation in the positive direction was observed at 2 and 2.5 MHz curves, and other lower frequencies did not exceed ±1 HMAX. Again, lift-off will be the significant factor at higher frequencies using the A3 probe. Overall, the A1 trendlines of HMAX are similar to VMAX deviated in a positive direction, which confirms the design characteristics of a probe. A wider frequency range similarly caused deviation of curves in both directions, mainly in the case of the A3 probe.

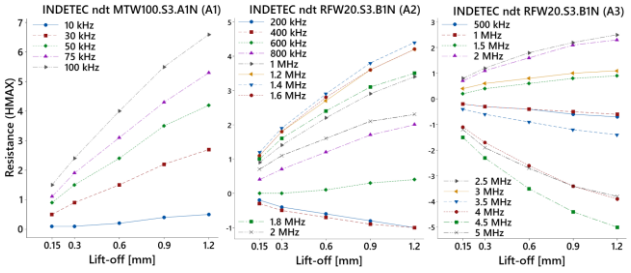

Figure 4. Resistance (HMAX) dependency on lift-off

It is more important to evaluate the lift-off influence with mutually expressed deviations of VMAX and HMAX parameters for each probe. The following Fig. 5 depicts the lift-off effect diagram of the A1 probe. A measurement was conducted at the intensification of the signal at 43 dB on both axes (VGAIN/HGAIN), and the phase angle was set at 208° using the ANGLE function. During such evaluation of probe identification abilities at its whole frequency range, the phase angle parameter is not such significant. The angle was set for each probe approximately to reach a similar development of curves at increasing frequency. It is evident that the ratio between the maximal VMAX and HMAX deviations is unbalanced, where higher HMAX values are present. It is known that this

parameter is more influenced by the lift-off variation and vice versa, VMAX is more sensitive to the material parameters, such as electrical conductivity, magnetic permeability, or various defects. Low conductivity of Inconel 718 alloy caused a lower maximal deviation of 2.2 VMAX at 10 kHz frequency with its decrease mainly below the 50 kHz frequency. Considering the overall lift-off shape of the A1 probe, lower sensitivity and resolution of defects at the expense of greater penetration depth can be expected.

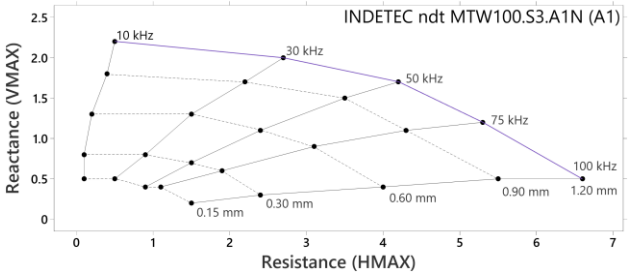

Figure 5. Lift-off effect diagram of A1 probe

A lift-off effect diagram of the A2 probe is included in the following Fig. 6. A measurement was conducted at 42 dB VGAIN/HGAIN and 115° ANGLE. The overall shape of the diagram is more balanced than in the case of the A1 probe and it covers a wider area due to the wider frequency range. The lowest deviation is present at low frequencies between 200 kHz – 800 kHz, but at such setting of parameters, the VMAX variation is the most significant at 600 kHz. HMAX deviation is the most significant at 1.4 MHz frequency. It can be stated that more detailed results of identification can be obtained using the higher frequencies, whereas, at the appropriate setting of gain parameters, 200 – 800 kHz can provide certain information about Inconel 718 alloy in shallower subsurface layers. Overall, the frequency curves of the A2 lift-off diagram are stronger at higher frequencies which is the consequence of a wider frequency range. A coil has predispositions for measurements using lower frequencies, but they cannot be such detailed as in the case of higher ones. Hence, the coil has certain restrictions in the covering of such a wider range.

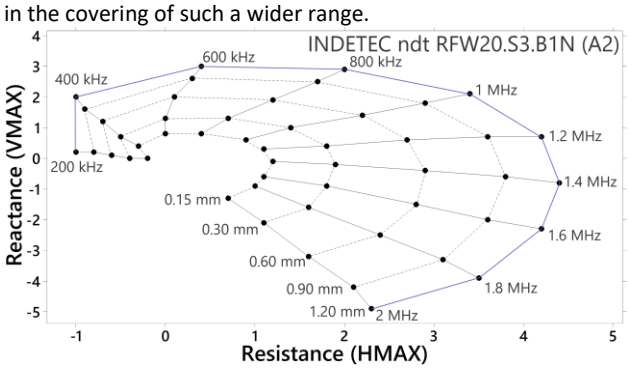

Figure 6. Lift-off effect diagram of A2 probe

The last A3 probe was tested at the setting of 44.5 dB VGAIN/HGAIN and 80° ANGLE (Fig. 7). Not negligible frequency range caused very inconspicuous deviation of 500 kHz on both axes and the wide range is also confirmed by the occupied area of a diagram. Greater deviations appeared above 2 MHz frequency with the gradual growth of curves up to the higher limit of the probe. The most deviated on the HMAX axis is the 4.5 MHz frequency curve and the most deviated on the VMAX axis is 5MHz curve. These higher frequencies can be suitable for the evaluation of a thin material surface layer, hence they have potential for special application, such as residual stress or density evaluation. The A3 probe works with the highest frequency range, which manifested more significantly in the form of weaker curves of lower frequencies due to the restriction of the coil to cover such a range.

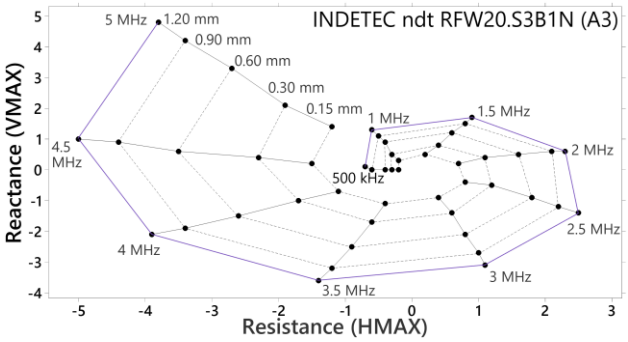

Figure 7. Lift-off effect diagram of A3 probe

4 DISCUSSION

The importance of this preliminary experiment is substantiated by the obtained resulting data which are necessary for setting up future ECT research on Inconel alloys, and it can be supplemented by findings from other studies. For example, the maximal calculated δ for the same A1 probe into the AM aluminium AlSi10Mg alloy was 1.05 mm [Geľatko 2024] and into the AM SS 316L stainless steel was 3.58 mm [Geľatko 2022], whereas in this experiment the value was on 6.61 mm for Inconel 718 alloy. These various values indicate that is highly important to calculate standard penetration depths for specific materials, which will be tested with the same probe. The A1 lift-off diagram confirms the prediction of its use for the lower-sensitivity application. Reversibly, A2 and A3 probes were selected due to the lower electrical conductivity of examined Inconel 718 alloy and it was confirmed with related lift-off diagrams, that these probes will be suitable for higher-sensitivity applications. Similarly, higher frequencies (30-1000 kHz) were used within the study [Guo 2021] and defects in the subsurface layers were detected using the 170 kHz, due to the higher penetration depth of lower frequencies (skin effect), which confirms predictions for the usability of probes in this experiment and their selection for the research. Lift-off effect is an important parameter for the expression of the identification abilities of the probe, whereas its evaluation was conducted within various experiments on aluminium and stainless steel [Spurek 2021], titanium [Du 2018], or nickel-based [Machado 2024] materials. Its overall shape is similar in various applications of the mentioned studies and within this experiment, but the magnitude of influencing the resistance and reactance is variable for different materials and probes, what is the reason for its evaluation before the specific identification, and it directly defines its importance.

5 CONCLUSIONS

The described preliminary study presents results for the preparation of crucial eddy-current testing parameters of Inconel 718 alloy through the expression of lift-off effect diagrams related to three selected probes and the calculation of standard penetration depth in their frequency range. The following conclusions can be stated:

- The electrical conductivity of Inconel 718 alloy was determined on the value of 1% IACS, which is less than the value of the data sheet (1.42% IACS), which confirms the necessity of measuring the conductivity for a specific material during the preparation of

experiment. Such behavior of material deserves other subsequent experiments.

- The standard penetration depth of the examined excitation frequency range is between 0.25 and 5.54 mm for the data sheet value of conductivity and between 0.3 and 6.61 mm for determined conductivity. Such difference of depth within the ECT is not negligible and needs to be considered before the identification.
- Reactance (VMAX) and resistance (HMAX) deviations based on lift-off variation at certain parameters were expressed for selected three probes. These parameters are important for the understanding of lift-off influence on the imaginary (VMAX) and the real (HMAX) part of overall coil resistance and for the creation of lift-off diagrams.
- Lift-off effect diagrams were described, whereas the A1 probe has smaller identification abilities, due to the lower frequency range within the lift-off diagram and lower usable frequencies (lower sensitivity) in comparison with the other two probes. Hence, it has predispositions for the identification of subsurface defects, due to the satisfactory sensitivity in its whole frequency range. It includes larger pores, porosity clusters, cracks, or more expanded delamination situated in deeper volumes of Inconel 718 alloy, with respect to calculated standard penetration depth.
- Higher frequencies of A2 and A3 probes had more significant deviations and tend to be more suitable for the applications with required higher sensitivity, which naturally grows with the frequency, which is proven by lift-off diagrams. Thus, they can be used for the identification and resolution of smaller surface pores, or cracks in shallow subsurface layers (up to 0.3 mm depth at maximal 5 MHz frequency), or a distinguishing of specimens based on different densities, residual stresses, changes of microstructure which are related to smaller dimensions where sensitivity of system is indispensable.

The experiment represents an important stepping stone for the setting of identification parameters related to the evaluation of Inconel 718 alloy using the ECT method and the creation of various methodologies for various purposes of non-destructive testing. Future related experiments need to be conducted on various artificial defects and varied material properties for both, subtractive manufactured and additive manufactured material Inconel 718. It is important to design artificial surface-reaching and sub-surface defects, representing commonly occurring discontinuities (cracks, porosity, delamination, etc.), evaluate the ECT signal characteristics as calibration indicators, express the recommended setting of parameters on a measurement device, and characterize the selection of certain probe, with the following verification on real discontinuities.

ACKNOWLEDGMENTS

This work was funded by the Slovak Research and Development Agency under contract No. APVV-21-0228 and the projects VEGA 1/0391/22 and KEGA 017TUKE-4/2023 were granted by the Ministry of Education, Science, Research and Sport of the Slovak Republic. This article is the result of the following project implementation: Development of excellent research capacities in the field of additive technologies for the Industry of the 21st century, ITMS: 313011BWN5, supported by the Operational Program Integrated Infrastructure funded by the ERDF.

REFERENCES

[Camerini 2018] Camerini, C., et al. In-line inspection tool with eddy current instrumentation for fatigue crack detection. Sensors, 2018, Vol.18, No.7, 2161. https://doi.org/10.3390/s18072161

[De Bartolomeis 2021] De Bartolomeis, A., et al. Future research directions in the machining of Inconel 718. Journal of Materials Processing Technology, 2021, Vol.297, 117260. https://doi.org/10.1016/j.jmatprotec.2021.117260

[Du 2018] Du, W., et al. Eddy current detection of subsurface defects for additive/subtractive hybrid manufacturing. The International Journal of Advanced Manufacturing Technology, 2018, Vol.95, pp 3185-3195. https://doi.org/10.1007/s00170-017-1354-2

[Evident 2025] Evident Olympus. NORTEC 600 User's Manual [online]. 2025. Available from https://industrial.evidentscientific.com.cn/en/downloads/detail/?0[downloads][id]=276825861.

[Farag 2022] Farag, H. E., et al. Non-destructive testing using eddy current sensors for defect detection in additively manufactured titanium and stainless-steel parts. Sensors, 2022, Vol.22, No.14, 5440. https://doi.org/10.3390/s22145440

[Garcia-Martin 2011] Garcia-Martin, J., et al. Non-destructive techniques based on eddy current testing. Sensors, 2011, Vol.11, No.3, pp 2525-2565. https://doi.org/10.3390/s110302525

[Geľatko 2022] Geľatko, M., et al. Eddy current testing of artificial defects in 316L stainless steel samples made by additive manufacturing technology. Materials, 2022, Vol. 15, No. 19, 6783. https://doi.org/10.3390/ma15196783

[Geľatko 2024] Geľatko, M., et al. Study of Eddy Current Testing Ability on SLM Aluminium Alloy. Materials, 2024, Vol.17, No.14, 3568. https://doi.org/10.3390/ma17143568

[Guo 2021] Guo, S., et al. Subsurface defect evaluation of selective-laser-melted inconel 738LC alloy using eddy current testing for additive/subtractive hybrid manufacturing. Chinese Journal of Mechanical Engineering, 2021, Vol.34, pp 1-16. https://doi.org/10.1186/s10033-021-00633-9

[Inkosas 2025] Inkosas. HAYNES® 718 alloy [online]. 2025. Available from https://www.inkosas.cz/download/niklove-slitiny/haynes-718.pdf.

[Krysztofik 2019] Krysztofik, J., et al. Evaluation of damage degree of Inconel 718 alloy with the use of non-destructive methods. Russian Journal of Nondestructive Testing, 2019, Vol.55, pp 299-307. https://doi.org/10.1134/S1061830919040107

[Machado 2024] Machado, M. A. Eddy currents probe design for NDT applications: A review. Sensors, 2024 Vol.24, No.17, pp 5819. https://doi.org/10.3390/s24175819

[Matweb 2025] Matweb. Copper, Cu; Annealed [online]. 2025. Available from https://www.matweb.com/search/datasheet.aspx?matguid=9aebe83845c04c1db5126fada6f76f7e.

[Matweb 2025] Matweb. Aluminum 7075-T6 [online]. 2025. Available from https://www.matweb.com/search/DataSheet.aspx?MatGUID=4f19a42be94546b686bbf43f79c51b7d.

[Mostafaei 2023] Mostafaei, A., et al. Additive manufacturing of nickel-based superalloys: A state-of-the-art review on process-structure-defect-property relationship. Progress in Materials Science, 2023, Vol.136, pp 101108. https://doi.org/10.1016/j.pmatsci.2023.101108

[Pereira 2014] Pereira, D., Clarke, T. G. Modeling and design optimization of an eddy current sensor for superficial and subsuperficial crack detection in inconel claddings. IEEE Sensors Journal, 2014, Vol.15, No.2, pp 1287-1292. https://doi.org/10.1109/JSEN.2014.2362072

[Spurek 2021] Spurek, M. A., et al. Relative density measurement of PBF-manufactured 316L and AlSi10Mg samples via eddy current testing. Metals, 2021, Vol.11, No.9, 1376. https://doi.org/10.3390/met11091376

[Spurek 2025] Spurek, M. A., et al. Influence of part temperature on in-situ monitoring of powder bed fusion of metals using eddy current testing. Progress in Additive Manufacturing, 2025, Vol.10, No.1, pp 15-32. https://doi.org/10.1007/s40964-024-00600-5

[Sun 2023] Sun, W., et al. Quality assessment of SUS316L fabricated by metal additive manufacturing with eddy current inspection. NDT & E International, 2023, Vol.138, pp 102901. https://doi.org/10.1016/j.ndteint.2023.102901

[Tytko 2024] Tytko, G., et al. Eddy Current Testing in the Quantitive Assessment of Degradation State in MAR247 Nickel Superalloy with Aluminide Coatings. Journal of Nondestructive Evaluation, 2024, Vol.43, No.4, pp 112. https://doi.org/10.1007/s10921-024-01129-x

CONTACTS:

Eng. MSc. Matus Geľatko, PhD.

Technical University of Kosice, Faculty of Manufacturing Technologies with a seat in Presov

Sturova 31, 080 01 Presov, Slovakia

matus.gelatko@tuke.sk